

Graphene Oxide as a Pathogen-Revealing Agent: Sensing with a Digital-Like Response**

Eden Morales-Narváez, Abdel-Rahim Hassan, and Arben Merkoçi*

Food poisoning and waterborne diseases drastically affect public health worldwide. They lead to countless premature deaths and massive losses in productivity, implying costs of several billions of dollars to cover healthcare and other consequent expenses. Furthermore, in the long term, they can lead to severe chronic conditions, such as reactive arthritis, ocular damage, and kidney failure.^[1] Therefore, the ability to detect pathogens that cause outbreaks of food poisoning or waterborne diseases is fundamental for safeguarding public health.

As nanomaterials exhibit properties that are absent in their corresponding bulk materials, they offer extraordinary potential for applications in health care and the food industry, aside from other fields.^[2] Among the most promising of these nanomaterials are graphene and its derivatives, such as graphene oxide (GO), which have been heralded for their combination of mechanical, electronic, magnetic, optic, and thermal properties, and which are now enabling nanoscale technologies and applications.^[3] In particular, researchers in diagnostics and environmental monitoring have been exploring these materials in sensing applications.^[4]

Graphene is generally described as a one-atom-thick planar sheet of sp²-bonded carbon atoms that are arranged in a two-dimensional honeycomb lattice.^[3a] Graphene oxide, in which some of the constituent carbon atoms of the graphene lattice bear oxygenated functional groups, such as carboxyl (at the lattice edges), ester, hydroxyl, or epoxide moieties (on the basal plane of the lattice), exhibits a similar structure.^[5] Therefore, GO can be readily functionalized with biomole-

cules or with chemically or electronically heterogeneous moieties, subsequently processed in solution, and selectively tuned for use as an insulator, semiconductor, or semi-metal.^[6] As an oxygenated lattice of donor and acceptor molecules exposed in a planar surface, GO is an excellent optical biosensing platform for detecting biological analytes, including DNA, cancer biomarkers, and viruses.^[7] Its photoluminescence has been exploited in microarray technologies for detecting rotaviruses, DNA, microcystins, and heavy-metal ions.^[8]

Another material that is used in sensing applications is quantum dots (QDs); these are semiconductor nanocrystals whose photonic properties are advantageous for sensing.^[9] Their properties include size-tunable emission, narrow and symmetric photoluminescence, broad and strong excitation spectra, strong luminescence, and robust photostability.^[10]


Fluorescence resonance energy transfer (FRET) is the transfer of photoexcitation energy from a donor fluorophore to an acceptor molecule. The efficiency of this photonic process mainly depends on the distance between donor and acceptor.^[11] Using theoretical calculations, Swathi and Sebastian determined that graphene could act as a highly efficient quencher of fluorophores. They calculated that quenching of FRET fluorescence using graphene would be observable up to a distance of approximately 300 Å,^[12] whereas FRET is typically observable at about 20–60 Å.^[11] Recently, Gaudreau and co-workers experimentally demonstrated that the high efficiency of energy transfer is predominantly due to the two-dimensionality of graphene and to its lack of gaps.^[13] In spite of being a disrupted lattice of sp²-bonded carbon atoms, GO can exhibit similar behavior. Interestingly, in studies in which GO was used as the acceptor, quenching was observable at distances greater than 20 nm.^[14]

Graphene oxide has been reported to be a universal highly efficient long-range quencher of fluorescence.^[7] Our group previously reported the extraordinary performance of GO as a quencher of QD fluorescence emission in the solid phase.^[15]

Herein, we report the design, fabrication, and testing of a novel pathogen-detection system based on antibody quantum dot (Ab-QD) probes, in which GO is employed as a pathogen-revealing agent (based on its quenching performance). To the best of our knowledge, this is the first report of using GO in the solid phase as an acceptor of energy transfer for biosensing. The system uses Ab-QD microarrays for pathogen attachment. The pathogen is selectively captured onto the Ab-QD probes, which fluoresce when excited with a laser, and then GO is added. In the presence of the pathogen, the (bound) probes barely interact with GO;

[*] Dr. E. Morales-Narváez, Dr. A.-R. Hassan, Prof. Dr. A. Merkoçi
Nanobioelectronics & Biosensors Group
Catalan Institute of Nanoscience and Nanotechnology
Barcelona, 08193 (Spain)
E-mail: arben.merkoci@icn.cat
Homepage: <http://nanobiosensors.org>
Dr. E. Morales-Narváez
ESAI department, Polytechnic University of Catalonia
Barcelona, 08028 (Spain)
Prof. Dr. A. Merkoçi
ICREA
Barcelona, 08010 (Spain)

[**] This work was supported by MICINN (Spain; MAT2011-25870) and by a CONACYT (Mexico) fellowship (E.M.-N.).

 Supporting information (details on reagents, fabrication of antibody-quantum dot microarrays, study of the transduction system, selective pathogen attachment and screening using GO, pathogen screening by sandwich immunoassays, amino-functionalization of silicon slides, SEM imaging, bacterial strains, and inoculum preparation) for this article is available on the WWW under <http://dx.doi.org/10.1002/anie.201307740>.

consequently, GO only minimally quenches their fluorescence.

However, in the absence of the pathogen, the (free) probes extensively interact with GO through π - π stacking, and GO quenches their fluorescence. The nano-enabled system and its operational mechanism are illustrated in Figure 1. As a model pathogen to test the system, we employed *Escherichia coli* O157:H7.^[16] We also tested the system in another configuration, in which Cy3-labelled antibodies, rather than GO, were used as the pathogen-revealing agent. The QDs employed were (core-shell) CdSe@ZnS QDs

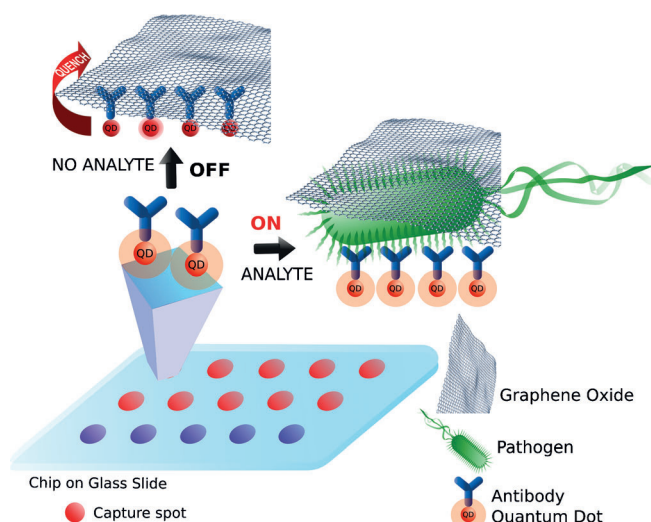


Figure 1. Operational concept of the nano-enabled system (illustration not to scale). The system relies on Ab-QD microarrays as a pathogen-attachment mechanism. Once the pathogen is selectively captured onto the Ab-QD probes (which can be excited with a laser), they are coated with GO platelets that reveal the presence of the pathogen. In the presence of the pathogen, the quenching of the probes is minimal, as they barely interact with GO (ON state), whereas in the absence of the pathogen, the probes are quenched by electrostatic or π - π stacking interactions between the probes and GO (OFF state).

that were functionalized with streptavidin. In previous characterization studies,^[17] we determined that these QDs are shaped like rice grains and have an average size of approximately 14 ± 2 nm. They also display a narrow emission spectrum (maximum peak: 655 nm) and a broad, strong excitation spectrum (from the UV to the visible (red) region). As GO, we employed GO platelets (Angstrom Materials Inc., Ohio, USA), with an elemental composition of 46 % carbon, 46 % oxygen, 3 % hydrogen, and 0.5 % nitrogen (manufacturer's data; w/w; approximate values). The platelets have lateral dimensions of approximately 180–1200 nm and an average thickness of approximately 1.1 nm; thus, a significant proportion of them comprise a single layer of GO. In water, they form a dark, amber-colored, non-aggregated colloidal suspension.

We ascertained the performance of the GO platelets as FRET acceptors of photons that were donated by Ab-QDs in the solid phase. In FRET, the fraction of photons that are absorbed by the donor and subsequently transferred to the acceptor can usually be increased by increasing the number of acceptor molecules;^[18] therefore, we performed our studies at different concentrations of GO.

We printed Ab-QD complexes in microspots of approximately 140 ± 10 μm , and then assayed quenching of their fluorescence by GO at different GO concentrations. As in microarray technology, the interaction of the spotted probes (in our system, Ab-QDs) and the molecule that is to be attached onto the probes (in our system, GO) strongly depends on both the concentration and the incubation time;^[19] therefore, we first studied the concentration and time dependence of the quenching (Figure 2). A calibration curve obtained from the quenching of the Ab-QD microarrays by GO at different concentrations (0 – 350 $\mu\text{g mL}^{-1}$) at an incubation time of 30 min yielded a linear response (Figure 2a',b); however, at an incubation time of 75 min, the response was exponential (Figure 2a'',b). These results indicate that an increase in GO concentration and an increase in the incubation time can both induce an increase in

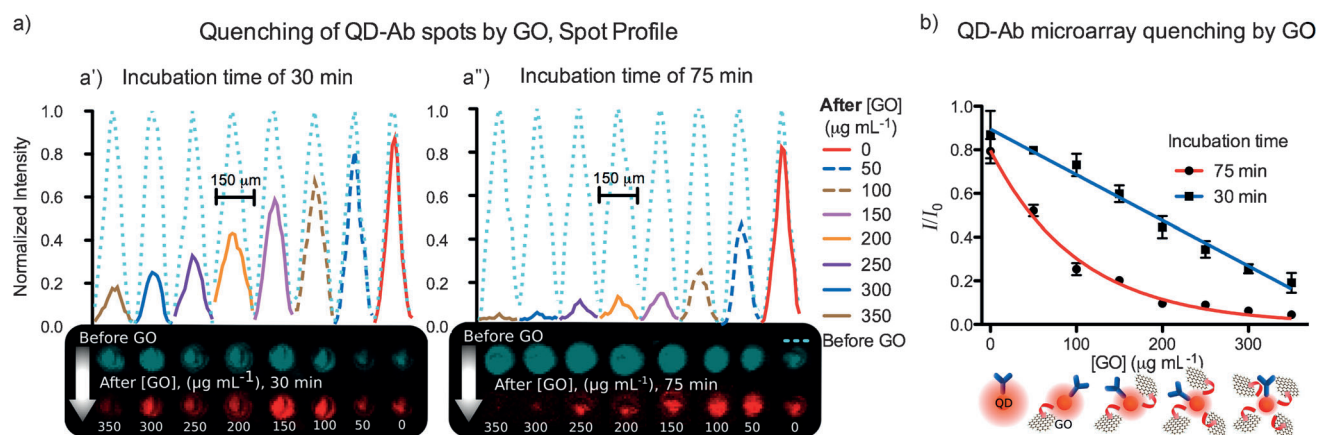


Figure 2. Transduction system performance. Concentration and time dependence of the quenching of Ab-QD microspots by GO. a) Spot profile of the quenching of Ab-QD microspots at different GO concentrations (0 – 350 $\mu\text{g mL}^{-1}$) at incubation times of 30 min (a') and 75 min (a''). The original profile of the explored spots (---) is also shown. Other plots indicate the final profiles of the observed spots. b) Calibration curves for the quenching experiment, using the same GO concentrations and the same incubation times. The error bars were calculated from a parallel assay of ten microspots. I/I_0 : final intensity/original intensity.

quenching efficiency. For example, at a GO concentration of approximately $350\ \mu\text{g mL}^{-1}$, an incubation time of 30 min gave a quenching efficiency of about 81%, whereas an incubation time of 75 min gave a quenching efficiency of approximately 96%. Blank incubations exhibited a quenching efficiency of about 20%; this effect was likely caused by microenvironmental changes in the assay (including changes in pH, humidity, ionic strength that are due to the washing and drying steps).^[10]

For this type of biosensing systems, one must account for any possible (undesired) interactions between the graphene material and the biomolecule analyte.^[20] For instance, non-covalent interactions between aromatic rings have been widely documented;^[21] these include the well-known π - π stacking interactions of GO with DNA strands.^[7,22] In our system, the hexagonal carbon rings in GO likely interact (non-covalently) with the aromatic amino acids in the antibody. Moreover, because of its oxygen-containing functional groups, GO can non-covalently interact with the diol, amino, and phenyl moieties in biomolecules.^[23] In fact, π - π stacking interactions between GO and nanoparticle-antibody structures have been reported for colloidal systems (liquid phase).^[24] In our system (solid phase), we observed strong interactions between the spotted Ab-QD probes and GO, which we characterized by Scanning Electron Microscopy (SEM). A SEM image of Ab-QD complexes inside a microspot and a SEM image of Ab-QDs/GO complexes inside a microspot are shown in Figure 3a and 3b, respectively (for experimental details, see the Supporting Information).

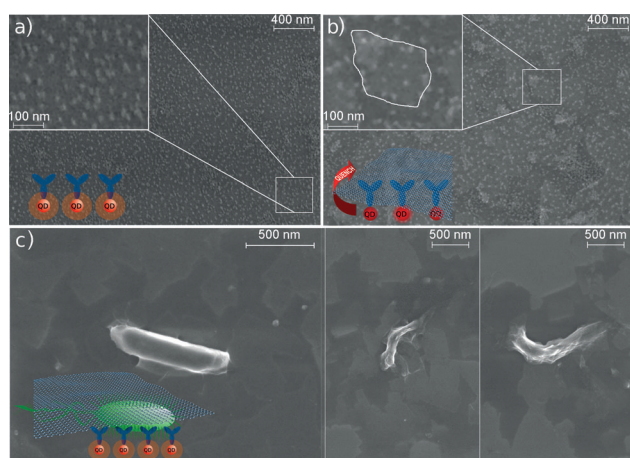


Figure 3. SEM images of the explored system. a) Ab-QD complexes inside a microspot. b) Ab-QD/GO complexes inside a microspot. c) Ab-QD/*E. coli* (membrane-bound)/GO complexes inside a microspot. Aminosilane silicon slides were used as the substrate.

We again printed Ab-QD probes in microspots of approximately $140 \pm 10\ \mu\text{m}$, and then monitored their interaction with *E. coli* O157:H7 as the target pathogen, at different concentrations of *E. coli* (5 – $10^7\ \text{CFU mL}^{-1}$; CFU = colony-forming unit; see the Supporting Information). Owing to a high density of functional groups, GO can interact with bacteria, resulting in bacterial cell deposition.^[25] The pathogen samples were assayed in phosphate-buffered saline (PBS)

supplemented with Tween 20 (0.05%, v/v). The Ab-QD spots were incubated with GO and subsequently became coated with GO, likely because of electrostatic or π - π stacking interactions. SEM images of *E. coli* cells (and cell fragments) that were pre-attached (through their membranes) to Ab-QD probes and then covered with GO platelets are shown in Figure 3c.

We expected that low concentrations of GO platelets would lead to light or disperse coatings, whereas high concentrations of GO platelets would lead to dense coatings. As the analyte was a few microns large (i.e., beyond the nanoscale), and the FRET effect is observable up to 30 nm, we reasoned that under optimal conditions, a small amount of analyte below a light or disperse coating might already be sufficient for preventing the energy transfer between the fluorescent spots and the GO platelets. In fact, Akhavan et al. have reported that the peak-to-valley distance around bacteria trapped within GO platelets can reach approximately 45 nm.^[26]

Given the aforementioned results, we concluded that our system, once optimized, would be able to display an ON/OFF (digital-like) response. When we used a high concentration of GO ($< 110\ \mu\text{g mL}^{-1}$) as the pathogen-revealing agent (which led to a dense coating of GO platelets), we were unable to distinguish between the absence and presence of the pathogen, as the quenching levels were similarly high in the two cases (see the Supporting Information, Figure S1). In contrast, when we used a low concentration of GO ($< 40\ \mu\text{g mL}^{-1}$), the probes were scarcely quenched (Figure 2b). Thus, we determined that the optimal conditions for the use of GO were an incubation time of 75 min and a GO concentration of approximately $70\ \mu\text{g mL}^{-1}$. In the absence of the target pathogen, the spotted probes were quenched by adding GO (blank signal).

As mentioned above, SEM images of the interacting components are shown in Figure 3a and b. Under optimal conditions, the system exhibits a transition at an *E. coli* concentration of approximately $10\ \text{CFU mL}^{-1}$ and becomes saturated at an *E. coli* concentration of about $10^7\ \text{CFU mL}^{-1}$ (see below). However, in the *E. coli* concentration range of 10^2 – $10^6\ \text{CFU mL}^{-1}$, the probes are scarcely quenched relative to the control signal (probes only, incubated with blanks throughout the assay; see Figure 4). As a threshold value for the limit of detection (LOD), we proposed to use the mean value of the blank signal, plus three times the standard deviation of the blank signal ($m_B + 3\sigma_B$).

To demonstrate the specificity of our system, we also assayed *Salmonella typhimurium* as a non-target pathogen. A small difference between blank incubations and the non-target pathogen incubations was observed, which was probably due to slight cross-reactivity between the probes and the non-target pathogen. Nevertheless, in the presence of *Salmonella typhimurium*, the quenching of the Ab-QD probes barely exceeded the proposed LOD (Figure 4b).

To explore the behavior of our system in a matrix other than PBS, we analyzed the target pathogen at several concentrations (3 – $10^7\ \text{CFU mL}^{-1}$) in tap-water samples. Interestingly, the system exhibited different quenching levels when PBS was used as matrix. This was probably due to changes in

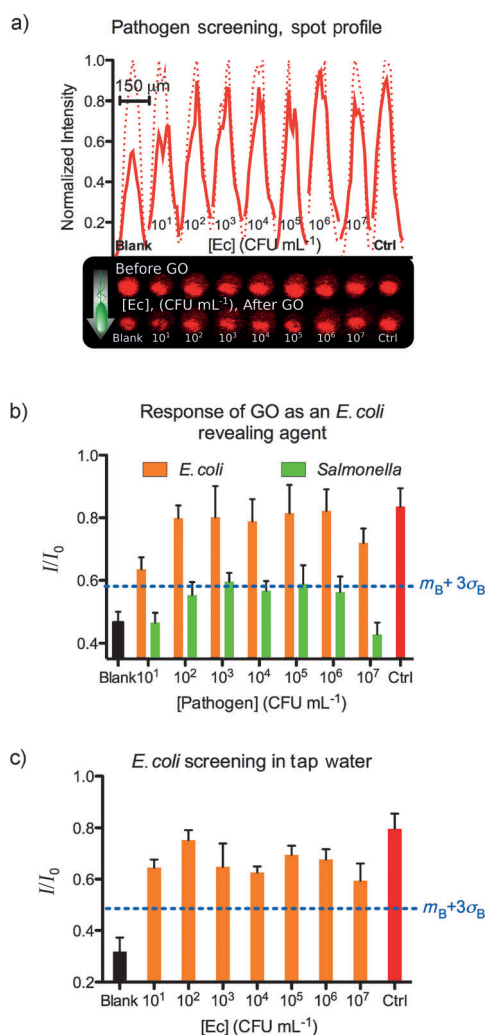


Figure 4. GO as a pathogen-revealing agent in an Ab-QD pathogen-detection system. a) Spot profile of the response of the system; original profile of the explored spots (.....); final profile of the observed spots at several *E. coli* concentrations after GO addition (—). b) In the absence of *E. coli*, the spots that comprise Ab-QD probes are quenched by adding GO (blank signal). In the presence of *E. coli*, the system exhibits a transition zone at [Ec] = 0–100 CFU mL⁻¹, becomes saturated at [Ec] = 10⁷ CFU mL⁻¹, and shows a constant signal at [Ec] = 10²–10⁶ CFU mL⁻¹, as the probes are scarcely quenched relative to the control signal. In the presence of a non-target pathogen (e.g., *Salmonella*), the quenching of the Ab-QD probes barely exceeds the proposed LOD ($m_B + 3\sigma_B$). c) *E. coli* screening in tap water. The error bars were typically obtained from parallel assays of ten microspots. I/I_0 : final intensity/original intensity.

the microenvironment, which typically affect the fluorescence quantum yield and the fluorescence decay behavior of QDs. Important aspects of the microenvironment include the polarity and hydrogen-bonding capability of the matrix and the local viscosity, pH, and ionic strength.^[10] The influence of the matrix was confirmed with the blank signal: The quenching in tap water occurred at an intensity ratio of 0.33, and at about 0.46 in PBS. Later, in the presence of the target pathogen (*E. coli*), the quenching in tap water was typically found at an intensity ratio of approximately 0.7 and at approximately 0.8 in PBS (Figure 4b,c and Figure S2).

However, despite the influence of microenvironmental changes, our system still enabled novel and qualitative pathogen detection in both matrices.

We then assessed the *E. coli* concentration at which our system would become saturated by performing a sandwich immunoassay of the spotted Ab-QD probes (for details, see the Supporting Information). In this configuration, we used Cy3-labeled antibodies, rather than GO, as the pathogen-revealing agent. The assay revealed that the system becomes saturated at approximately 10⁷ CFU mL⁻¹ (Figure 5 and Figure S3).

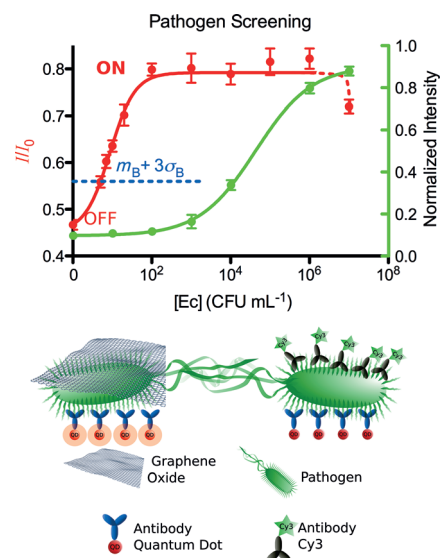


Figure 5. Towards a new generation of biosensors that give a digital-like response. An Ab-QD pathogen-detection system was tested in two configurations with *E. coli* as the target pathogen. In the standard configuration (GO as the pathogen-revealing agent), the system was highly sensitive and gave a digital-like (ON/OFF) response (—; approximated curve). In this configuration, the system exhibited a sharp transition zone (from the OFF state to the ON state) at very low *E. coli* concentrations. In contrast, in the sandwich immunoassay (using Cy3-labelled antibodies as the pathogen-revealing agent), the system gave an analog-type response (—), in which the signal gradually strengthened with increasing *E. coli* concentration. The error bars were obtained from parallel assays of 10 microspots in each configuration. LOD threshold (---): $m_B + 3\sigma_B$. I/I_0 : final intensity/original intensity.

In the standard configuration (with GO), our system gives a digital-like response: OFF indicates the absence of the pathogen (*E. coli*), and ON indicates the presence of it. However, in this configuration, the system exhibited a sharp transition zone from the OFF state to the ON state at very low concentrations of *E. coli* (ca. 10 CFU mL⁻¹). As we observed a similar response in the presence of *E. coli* regardless of its concentration (ca. 100–10⁷ CFU mL⁻¹), we consider this configuration to be qualitative.

Interestingly, in the sandwich immunoassay (i.e., using Cy3-labelled antibodies instead of GO), the system gives an analog-like response: The signal of Cy3 fluorescence gradually strengthens with increasing pathogen concentration, until the system becomes saturated. However, this configuration

did not give a clearly observable (strong) signal in an *E. coli* concentration range of $10\text{--}100\text{ CFU mL}^{-1}$ (Figure S3). Despite the lack of a clear signal in this range, there was still a small amount of bound analyte. In this context, the proposed GO configuration can reveal the bound analytes that are barely observable in the sandwich immunoassay, owing to the sensitive FRET phenomenon that the former is exploiting. The LOD of the sandwich immunoassay is approximately $3.8 \times 10^3\text{ CFU mL}^{-1}$; thus, the GO configuration is advantageous in terms of sensitivity (Figure 5).

Qualitative sensors might prove highly useful for diagnosis and other analytical applications.^[27] When used with GO, our pathogen-detection system is highly sensitive, exhibiting an LOD of approximately 5 CFU mL^{-1} for *E. coli* in PBS and in tap water (Figure 5 and Figure S2). As a potential diagnostic tool, this configuration might be extended to detect other types of analyte (e.g., cancer cells), perform other tasks (e.g., molecular logic operations),^[28] or be applied to other nanoscale biosystems.

Aside from its diverse properties described earlier, GO has also been reported to have strong antibacterial activity.^[25,29] In this context, the literature suggests that the cytotoxicity of GO depends on several parameters, such as concentration, incubation time, and the lateral size and the oxidation level of the GO platelets.^[29,30] Thus, as a possible branch of future research, we envision a biosensing and microbicidal GO-based system that would both detect and kill bacteria by compromising the integrity of the bacterial membrane.

Received: September 3, 2013

Published online: November 7, 2013

Keywords: biosensors · graphene oxide · microarrays · pathogens · resonance energy transfer

- [1] M. McKenna, *Sci. Am.* **2012**, 306, 26–27.
- [2] a) W. R. Sanhai, J. H. Sakamoto, R. Canady, M. Ferrari, *Nat. Nanotechnol.* **2008**, 3, 242–244; b) T. V. Duncan, *Nat. Nanotechnol.* **2011**, 6, 683–688; c) A. P. F. Turner, *Chem. Soc. Rev.* **2013**, 42, 3184–3196.
- [3] a) A. K. Geim, K. S. Novoselov, *Nat. Mater.* **2007**, 6, 183–191; b) D. Jariwala, V. K. Sangwan, L. J. Lauhon, T. J. Marks, M. C. Hersam, *Chem. Soc. Rev.* **2013**, 42, 2824–2860; c) J. van den Brink, *Nat. Nanotechnol.* **2007**, 2, 199–201; d) C. Cheng, D. Li, *Adv. Mater.* **2013**, 25, 13–30; e) D. Bitounis, H. Ali-Boucetta, B. H. Hong, D.-H. Min, K. Kostarelos, *Adv. Mater.* **2013**, 25, 2258–2268; f) Y. Zhu, D. K. James, J. M. Tour, *Adv. Mater.* **2012**, 24, 4924–4955; g) D. Wei, Y. Liu, *Adv. Mater.* **2010**, 22, 3225–3241.
- [4] a) L. Feng, L. Wu, X. Qu, *Adv. Mater.* **2013**, 25, 168–186; b) H. Y. Mao, S. Laurent, W. Chen, O. Akhavan, M. Imani, A. A. Ashkarran, M. Mahmoudi, *Chem. Rev.* **2013**, 113, 3407–3424; c) K. Yang, L. Feng, X. Shi, Z. Liu, *Chem. Soc. Rev.* **2013**, 42, 530–547.
- [5] a) S. Park, R. S. Ruoff, *Nat. Nanotechnol.* **2009**, 4, 217–224; b) J. T. Robinson, F. K. Perkins, E. S. Snow, Z. Wei, P. E. Sheehan, *Nano Lett.* **2008**, 8, 3137–3140.
- [6] K. P. Loh, Q. Bao, G. Eda, M. Chhowalla, *Nat. Chem.* **2010**, 2, 1015–1024.
- [7] E. Morales-Narváez, A. Merkoçi, *Adv. Mater.* **2012**, 24, 3298–3308.
- [8] a) J. H. Jung, D. S. Cheon, F. Liu, K. B. Lee, T. S. Seo, *Angew. Chem.* **2010**, 122, 5844–5847; *Angew. Chem. Int. Ed.* **2010**, 49, 5708–5711; b) F. Liu, J. Y. Choi, T. S. Seo, *Biosens. Bioelectron.* **2010**, 25, 2361–2365; c) Y. Shi, J. Wu, Y. Sun, Y. Zhang, Z. Wen, H. Dai, H. Wang, Z. Li, *Biosens. Bioelectron.* **2012**, 38, 31–36; d) F. Liu, H. D. Ha, D. J. Han, T. S. Seo, *Small* **2013**, 9, 3410–3414.
- [9] I. L. Medintz, H. T. Uyeda, E. R. Goldman, H. Mattoussi, *Nat. Mater.* **2005**, 4, 435–446.
- [10] U. Resch-Genger, M. Grabolle, S. Cavaliere-Jaricot, R. Nitschke, T. Nann, *Nat. Methods* **2008**, 5, 763–775.
- [11] P. R. Selvin, *Nat. Struct. Biol.* **2000**, 7, 730–734.
- [12] a) R. S. Swathi, K. L. Sebastian, *J. Chem. Phys.* **2008**, 129, 054703; b) R. S. Swathi, K. L. Sebastian, *J. Chem. Phys.* **2009**, 130, 086101.
- [13] L. Gaudreau, K. J. Tielrooij, G. E. D. K. Prawiroatmodjo, J. Osmond, F. J. G. de Abajo, F. H. L. Koppens, *Nano Lett.* **2013**, 13, 2030–2035.
- [14] T. N. Lin, L. T. Huang, G. W. Shu, C. T. Yuan, J. L. Shen, C. A. J. Lin, W. H. Chang, C. H. Chiu, D. W. Lin, C. C. Lin, H. C. Kuo, *Opt. Lett.* **2013**, 38, 2897–2899.
- [15] E. Morales-Narváez, B. Pérez-López, L. B. Pires, A. Merkoçi, *Carbon* **2012**, 50, 2987–2993.
- [16] a) S. Park, R. W. Worobo, R. A. Durst, *Crit. Rev. Food Sci. Nutr.* **1999**, 39, 481–502; b) J. C. Yarze, M. P. Chase, *Am. J. Gastroenterol.* **2000**, 95, 1096.
- [17] E. Morales-Narváez, H. Montón, A. Fomicheva, A. Merkoçi, *Anal. Chem.* **2012**, 84, 6821–6827.
- [18] R. C. Somers, M. G. Bawendi, D. G. Nocera, *Chem. Soc. Rev.* **2007**, 36, 579–591.
- [19] W. Kusnezow, Y. V. Syagailo, S. Rüffer, K. Klenin, W. Sebal, J. D. Hoheisel, C. Gauer, I. Goychuk, *Proteomics* **2006**, 6, 794–803.
- [20] J. A. Mann, T. Alava, H. G. Craighead, W. R. Dichtel, *Angew. Chem.* **2013**, 125, 3259–3262; *Angew. Chem. Int. Ed.* **2013**, 52, 3177–3180.
- [21] G. B. McGaughey, M. Gagné, A. K. Rappé, *J. Biol. Chem.* **1998**, 273, 15458–15463.
- [22] a) C.-H. Lu, H.-H. Yang, C.-L. Zhu, X. Chen, G.-N. Chen, *Angew. Chem.* **2009**, 121, 4879–4881; *Angew. Chem. Int. Ed.* **2009**, 48, 4785–4787; b) B. J. Hong, Z. An, O. C. Compton, S. T. Nguyen, *Small* **2012**, 8, 2469–2476.
- [23] J.-L. Chen, X.-P. Yan, K. Meng, S.-F. Wang, *Anal. Chem.* **2011**, 83, 8787–8793.
- [24] a) L. Chen, X. Zhang, G. Zhou, X. Xiang, X. Ji, Z. Zheng, Z. He, H. Wang, *Anal. Chem.* **2012**, 84, 3200–3207; b) H. Zhao, Y. Chang, M. Liu, S. Gao, H. Yu, X. Quan, *Chem. Commun.* **2013**, 49, 234–236.
- [25] S. Liu, T. H. Zeng, M. Hofmann, E. Burcombe, J. Wei, R. Jiang, J. Kong, Y. Chen, *ACS Nano* **2011**, 5, 6971–6980.
- [26] O. Akhavan, E. Ghaderi, A. Esfandiari, *J. Phys. Chem. B* **2011**, 115, 6279–6288.
- [27] A. P. F. Turner, N. Magan, *Nat. Rev. Microbiol.* **2004**, 2, 161–166.
- [28] A. P. de Silva, S. Uchiyama, *Nat. Nanotechnol.* **2007**, 2, 399–410.
- [29] O. Akhavan, E. Ghaderi, *ACS Nano* **2010**, 4, 5731–5736.
- [30] a) S. Liu, M. Hu, T. H. Zeng, R. Wu, R. Jiang, J. Wei, L. Wang, J. Kong, Y. Chen, *Langmuir* **2012**, 28, 12364–12372; b) S. Das, S. Singh, V. Singh, D. Joung, J. M. Dowling, D. Reid, J. Anderson, L. Zhai, S. I. Khondaker, W. T. Self, S. Seal, *Part. Part. Syst. Charact.* **2013**, 30, 148–157.